RADIATION RESEARCH **184**, 352–366 (2015)
0033-7587/15 $15.00

DOI: 10.1667/RR14047.1

Long-Lasting Impact of Neonatal Exposure to Total Body Gamma Radiation on Secondary Lymphoid Organ Structure and Function

Javier Rangel-Moreno,[a,1] Maria de la Luz Garcia-Hernandez[a,1] Rosalio Ramos-Payan,[a] Jamie Biear,[a] Eric Hernady,[b] Mark Y. Sangster,[c] Troy D. Randall,[f] Carl J. Johnston,[d] Jacob N. Finkelstein[b,d] and Jacqueline P. Williams[b,e,2]

Departments of [a] Medicine, [b] Environmental Medicine, [c] Microbiology and Immunology, [d] Pediatrics and Neonatology and [e] Radiation Oncology, University of Rochester Medical Center, Rochester, New York; and [f] Division of Clinical Immunology and Rheumatology, University of Alabama at Birmingham, Birmingham, Alabama

Rangel-Moreno, J., de la Luz Garcia-Hernandez, M., Ramos-Payan, R., Biear, J., Hernady, E., Sangster, M. Y., Randall, T. D., Johnston, C. J., Finkelstein, J. N. and Williams, J. P. Long-Lasting Impact of Neonatal Exposure to Total Body Gamma Radiation on Secondary Lymphoid Organ Structure and Function. *Radiat. Res*. 184, 352–366 (2015).

The acute period after total body irradiation (TBI) is associated with an increased risk of infection, principally resulting from the loss of hematopoietic stem cells, as well as disruption of mucosal epithelial barriers. Although there is a return to baseline infection control coinciding with the apparent progressive recovery of hematopoietic cell populations, late susceptibility to infection in radiation-sensitive organs such as lung and kidney is known to occur. Indeed, pulmonary infections are particularly prevalent in hematopoietic cell transplant (HCT) survivors, in both adult and pediatric patient populations. Preclinical studies investigating late outcomes from localized thoracic irradiation have indicated that the mechanisms underlying pulmonary delayed effects are multifactorial, including exacerbated and persistent production of pro-inflammatory molecules and abnormal cross-talk among parenchymal and infiltrating immune and inflammatory cell populations. However, in the context of low-dose TBI, it is not clear whether the observed exacerbated response to infection remains contingent on these same mechanisms. It is possible instead, that after systemic radiation-induced injury, the susceptibility to infection may be independently related to defects in alternative organs that are revealed only through the challenge itself; indeed, we have hypothesized that this defect may be due to radiation-induced chronic effects in the structure and function of secondary lymphoid organs (SLO). In this study, we investigated the molecular and cellular alterations in SLO (i.e., spleen, mediastinal, inguinal and mesenteric lymph nodes) after TBI, and the time points when there appears to be immune competence. Furthermore, due to the high incidence of pulmonary infections in the late post-transplantation period of bone marrow transplant survivors, particularly in children, we focused on outcomes in mice irradiated as neonates, which served as a model for a pediatric population, and used the induction of adaptive immunity against influenza virus as a functional end point. We demonstrated that, in adult animals irradiated as neonates, high endothelial venule (HEV) expansion, generation of follicular helper T cells (TFH) and formation of splenic germinal centers (GC) were rapidly and, more importantly, persistently impaired in SLO, suggesting that the early-life exposure to sublethal radiation had long-lasting effects on the induction of humoral immunity. Although the neonatal TBI did not affect the overall outcome from influenza infection in the adults at the earlier time points assessed, we believe that they nonetheless contribute significantly to the increased mortality observed at subsequent late time points. Furthermore, we speculate that the detrimental and persistent impact on the induction of CD4 T- and B-cell responses in the mediastinal lymph nodes will decrease the animals' ability to respond to other aerial pathogens. Since many of these pathogens are normally cleared by antibodies, our findings provide an explanation for the susceptibility of survivors of childhood HCT to life-threatening respiratory tract infections. These findings have implications regarding the need for increased monitoring in pediatric hematopoietic cell transplant patients, since they indicate that there are ongoing and cumulative defects in SLO, which, importantly, develop during the immediate and early postirradiation period when patients may appear immunologically competent. The identification of changes in immune-related signals may offer bioindicators of progressive dysfunction, and of potential mechanisms that could be targeted so as to reduce the risk of infection from extracellular pathogens. Furthermore, these results support the potential susceptibility of the pediatric population to infection after sublethal irradiation in the context of a nuclear or radiological event.

INTRODUCTION

Total body irradiation (TBI) is frequently used as part of the preparatory regimen for hematopoietic cell transplantation (HCT) in both adult and pediatric patients. However,

[1] These authors contributed equally to this work.

[2] Address for correspondence: Department of Environmental Medicine, University of Rochester School of Medicine and Dentistry, 601 Elmwood Avenue, Box EHSC, Rochester, NY 14624; email: Jackie_Williams@urmc.rochester.edu.

beyond their myeloablative effects, sublethal doses of TBI can also cause acute and chronic damage in multiple organs and cell populations, possibly contributing to the range of morbidities observed in surviving HCT patient populations. For example, pediatric survivors of HCT can present with endocrinopathies, musculoskeletal disorders, cardiopulmonary compromise, graft-versus-host disease (GVHD), organ toxicity and increased susceptibility to infection (*1–4*). Late effects are particularly prevalent in the lung, observed as an increased sensitivity to respiratory tract infections (*5–7*), with some patients developing pulmonary effects similar to those associated with late injury from localized irradiation, such as pneumonitis and lung fibrosis (*8*). Although our group has previously demonstrated that TBI of neonate mice induces a progressive exacerbation of influenza-associated morbidity and mortality with age (*9*), it remains unknown whether this outcome was a direct effect of radiation exposure to the neonate lung or the result of systemic injury to the secondary lymphoid organ (SLO) structure and, as a result, impaired induction of adaptive influenza immunity in adult life.

Importantly with respect to this investigation, the various elements of the SLO respond differentially to insult across the age spectrum. For example, in the womb, interactions between lymphoid tissue inducer cells (LTi) and stromal cell organizers are key in the generation of the SLO scaffold (*10, 11*). Indeed, a decline in LTi numbers in fetuses reduces SLO size and impairs the later induction of protective immunity, as demonstrated in adult mice with respect to their response against gamma herpes viruses (*12*). With development into the neonatal stage, even though LTi are still seen in mice, postnatal SLO expansion relies on interactions between lymphocytes and stromal cells (*13*). For example, B cells induce differentiation of stromal cells into follicular dendritic cells (FDC) (*14*), which express CXC chemokine ligand 13 (CXCL13), a chemokine critical for maintaining B-cell follicle integrity. In T-cell areas, dendritic cells (DC) induce differentiation of blood vessels into high endothelial venules (HEV) (*15*), the portals for entry of rare antigen-specific naïve T cells into SLO. In the adult mouse, secondary lymphoid organs, such as spleen and lymph nodes, have distinctive and functional T- and B-cell domains that orchestrate highly regulated immune responses (*16*), and represent an important site for the amplification of chronic immune responses. The integrity and cell organization in the distinct B-cell and T-cell compartments is maintained by specific stromal follicular dendritic cells and fibroblastic reticular cells, respectively (*16*), which produce homeostatic chemokines that are the choreographers of B- and T-cell responses (*17*). In addition, the nonhematopoietic components in these organs play a role in infection response by forming important scaffold structures as well as a specialized network of conduits that are important in cell migration and antigen transport (*18*).

The ability of immune cells in adult lungs to respond quickly to microbial stimulation depends on the rapid induction of adaptive immunity in the mediastinal lymph nodes (MLN), which are critical for the timely recruitment of antigen-specific lymphocytes to the pulmonary tract and the accelerated clearance of aerial pathogens (*19*). Given the known radiation sensitivity of many of these cell types, we have hypothesized that depletion of lymphocytes by TBI during the early stages of life will affect the downstream structure of SLO, leading to a long-term impairment of immunity in response to infection. To test our hypothesis, we exposed 4-day-old C57BL/6 mice to a sublethal dose of TBI (5 Gy) and evaluated structural and functional changes in the SLO [MLN, inguinal (ILN) and mesenteric (MeLN) lymph nodes and spleen] at various time points postirradiation.

MATERIALS AND METHODS

Mice and Irradiation

C57BL/6 mice were acquired at 4 days old from an in-house breeding colony (original breeding pairs were acquired from Jackson Laboratories, Bar Harbor, ME) and remained with their dams in the animal facilities at the University of Rochester until weaning at 28 days postnatal. Animals were then caged by sex, 5 per cage and maintained on standard laboratory chow and hydrogels. All experiments were conducted in compliance with institutional animal guidelines. For radiation exposures, neonate animals were placed in custom-built Plexiglas jigs and 5 Gy TBI from a ^{137}Cs γ-ray source (JL Shepherd, San Fernando, CA), operating at a dose rate of approximately 1.7 Gy/min and then immediately returned to their dams. Control animals were sham irradiated.

Influenza Virus Infection

Sham-irradiated and irradiated 2- or 6-month-old C57BL/6 mice were anesthetized with isoflurane and intranasally inoculated with 1×10^4 egg infectious dose fifty (EID_{50}) of influenza A/HK/X31 (H3N2) in 100 μl of sterile phosphate buffered saline (PBS). Mock-infected groups received a similar volume of PBS. Mice were monitored every other day for changes in body weight, signs of distress and mortality associated with infection. On day 7, 10 or 14 after infection, mice were euthanized and their spleen, MLN, ILN and MeLN and lungs were collected for analysis.

Flow Cytometry

Cell suspensions were generated from lung and MLN as previously described (*20*). MLN, ILN and MeLN were collected in 4°C FACS buffer [2% fetal bovine serum (FBS) in PBS] and ground up using sterile metallic cell strainers. Lungs were digested with collagenase and DNase I for 30 min at 37°C and the residual lung tissue was then ground up using sterile metallic cell strainers. Cell suspensions were treated with lysis buffer (0.15 *M* NH_4Cl, 1 m*M* $NaHCO_3$, 0.1 m*M* EDTA) at room temperature for 5 min to eliminate red blood cells. Lysis solution was neutralized with cold FACS buffer and cells were spun at 1,800 rpm for 5 min. Leukocytes (1×10^6) were incubated with antibodies against Fc receptors at 4 μg/ml (CD16/CD32, 2.4G2; Bio X Cell, West Lebanon, NH) for 10 min, then stained with $NP_{366–374}/D^b$ class I (Trudeau Institute, Saranac Lake, NY) or $NP_{311–325}/I\text{-}A^b$ class II tetramers (kindly provided by the NIH tetramer facility, Emory University, Atlanta, GA) for 1 h at 4°C. In addition, single cell suspensions were stained with antibodies specific for one of the following to detect follicular helper T cells (TFH): CD3-APCeFluor780 (17A2), CD8a-PE (53-6.7), CD8-V500 (53-6.7), CD45R-V500 (RA3-6B2), CXCR5-biotin (2G8) (all from BD

Pharmingen™, San Jose, CA), CD279-FITC (PD1, J43; eBioscience Inc., San Diego, CA) or CD278-PerCPCy5.5 (ICOS, C398.4A; BioLegend® Inc., San Diego, CA). CD19-APC (1D3; BD Pharmingen), PNA-FITC and CD95-PeCy7 (Jo2; BD Pharmingen) were used to detect germinal center B cells. To define populations of $CD45^+$ hematopoietic cells, $CD45^-$ nonhematopoietic cells and lymphoid tissue inducer cells, CD45-FITC (30-F11; BD Pharmingen) was combined with a lineage-negative cocktail of: CD3-PECy5 (145-2C11), CD11b-PECy5 (M1/70), CD11c-PECy5 (N418), F4/80-PECy5 (BM8), Ly6C-Ly6G-PECy5 (Gr-1, RB6-8C5), NK1.1-PECy5 (PK136), all from BioLegend, as well as CD45R-PECy5 (B220, RA3-6B2; eBioscience) and CXCR5-biotin (2G8; BD Pharmingen). Cells were then washed twice with FACS media (PBS containing 2% FBS) and biotin-conjugated antibodies were detected with streptavidin-PE (554061; BD Pharmingen). Cells were then washed twice and resuspended in media containing 1 μg/ml of propidium iodide to eliminate dead cells from analysis. Foxp3 staining was performed with a PE-mouse/rat Foxp3 staining set, as recommended by manufacturers (e-Biosciences). A total of 10^5 live cells were collected in an LSRII flow cytometer (BD Biosciences) and data were analyzed with FlowJo software (Tree Star, Inc., Ashland, OR).

Live lymphocytes were selected based on FSC, SSC profile and the exclusion of propidium iodide; cells then were gated in CD3. $NP_{311–325}$/$I\text{-}A^b$ versus CD4 and $NP_{366–374}/D^b$ versus CD8 were plotted to detect $CD3^+NP^+$ CD4 and CD8 T cells. For TFH, we first selected live lymphocytes, followed by plotting CD3 against CD8-B220 to exclude $CD8^+$ T cells and $B220^+$ B cells from the analysis ($CD3^+CD8^-B220^-$ cells). Next, we selected double-positive $CD4^+CXCR5^+$ cells. Inside $CD3^+CD4^+CXCR5^+$ cells positive for both CD278 (ICOS) and CD279 (PD1) were considered TFH. Germinal center B (GCB) cells were defined as live $CD19^+$ cells that expressed CD95 (FAS) and bound peanut agglutinin. Live cells in spleen, MLN, ILN and MeLN and lungs were counted in a hemocytometer using the trypan blue exclusion method. The number of live cells was used to calculate the total number of effector lymphocytes per organ, based on the frequency for each cell population.

Immunofluorescence

Frozen tissue sections (5 μm) were blocked with antibodies against Fc receptors (2 μg/ml) for 30 min and incubated for 1 h with primary antibodies specific for CD3 (M-20; Santa Cruz Biotechnology®, Dallas, TX), biotin-CD21-CD35-biotin (7E9; BioLegend), CD45R-APC (B220, RA3-6B2; BD Pharmingen), followed by incubation with Alexa Fluor® 568-donkey anti-goat (A11057; Invitrogen, Grand Island, NY) and Alexa Fluor 488-streptavidin (S11223; Invitrogen) to visualize $CD3^+$ T cells, $CD21^-CD35^+$ FDC networks and $B220^+$ B cells, respectively. High endothelial venules, lymphatics and DC were detected with primary antibodies against PNAd (MECA-79; BD Pharmingen), Lyve 1 (DP3513; Acris Antibodies Inc., San Diego, CA) and CD11c-APC (HL3; BD Pharmingen). Unlabeled primary antibodies were detected with Cy3-goat anti-rat IgM (112-165-020; Jackson Immunoresearch Laboratories, West Grove, PA), and FITC donkey-anti-rabbit (711-096-152; Jackson Immunoresearch Laboratories). Germinal centers (GC) were visualized with antibodies specific for CD3 (M-20; Santa Cruz Biotechnology), in combination with PNA-FITC (L7381-1MG; Sigma-Aldrich® LLC, St. Louis, MO) and CD45R-APC (B220, RA3-6B2; BD Pharmingen). Primary antibodies for CD3 were detected with Alexa Fluor 568-donkey anti-goat (A11057; Invitrogen). CD4 T cells were detected with CD4-APC (RM4-5; BD Pharmingen). Tissue sections were then mounted using Prolong® Gold Antifade with DAPI (Invitrogen, San Diego, CA). Pictures were taken with a Zeiss Axioplan microscope and recorded with a Hamamatsu camera (Carl Zeiss, Thornwood, NY). All HEV in individual MLN sections or all GC in individual spleen sections were outlined with an automated tool of the Zeiss Axioplan software and the average HEV and GC sizes were calculated. After morphometric analysis, representative pictures were taken at 200× magnification.

RNA Extraction and Quantitative PCR

Total RNA was isolated using TRIzol® (Invitrogen) according to the manufacturer's instructions. Total DNA-treated RNA (3 μg) was reverse transcribed using random primers and SuperScript® II (Invitrogen). Quantitative PCR was performed using TaqMan® Universal PCR Master Mix, following the Applied Biosystems® protocol (Foster City, CA). All probes were purchased from Applied Biosystems: Cxcl9 (Mm00434946_m1), Cxcl10 (Mm00445235_m1), Cxcl11 (Mm00444662_m1), Cxcl13 (Mm04214185_s1), Ccl19 (Mm00839967_g1), collagen type I (Mm00801666_g1), fibronectin (Mm01256744_m1), fucosyl transferase VII (Mm04242850_m1) and complement receptor 2 (CD21, Mm00801681_m1). mRNA expression was first normalized to GAPDH and the fold change in mRNA expression for each specific gene in irradiated groups was compared to the expression levels in organs from 11-day-old or 2-month-old sham-irradiated mice using the ΔΔCt method.

Enzyme-Linked Immunosorbent Assay (ELISA)

Levels of influenza-specific antibodies were measured in serum as previously described (*21*). To collect serum, after euthanasia, the renal artery in each animal was severed with scissors, and blood was collected in a sterile 0.5 ml Eppendorf® tube. Tubes were incubated at room temperature for 30 min and tubes were spun at 5,000 rpm for 10 min. The serum was then transferred to 0.5 ml sterile Eppendorf tubes and frozen at −20°C until analyzed. Briefly, for analysis, ELISA plates were coated with heat/UV-inactivated influenza A/HK/X31, followed by incubation with serial dilutions of serum and developed with HRP-conjugated, goat anti-mouse IgG (1030-05; SouthernBiotech, Birmingham, AL). End point titer was calculated by interpolating the cutoff value of a 0.2 optical density into the titration curve.

Statistical Analysis

Data were analyzed with GraphPad Prism (GraphPad Software Inc., LaJolla, CA) and points represent the mean ± SEM. Statistical significance was calculated by two-tailed unpaired Student's *t* test and differences of $P < 0.05$ were considered statistically significant.

RESULTS

Acute Effects of Radiation on Neonatal SLO

Interactions between hematopoietic cells and stromal cell populations are critical for the expansion and organization of SLO during development (*13*). Therefore, any systemic injury that affects these cells during the neonatal period can have long-term effects on subsequent SLO function, including their ability to generate immune responses to antigens. Indeed, we have previously demonstrated a progressive exacerbation in morbidity and mortality in 6- and 9-month-old C57BL/6 mice exposed to radiation during the neonatal period and subsequently challenged with influenza virus (Table 1) (*9*). However, the irradiated animals challenged at 3 months with influenza exhibited complete resolution and normal recovery from the viral infection (Table 1), suggesting that there may be a latent period in the onset and progression of defect development in this system.

Mitigating strategies are, by definition, delivered prior to symptomatic disease. In an effort to identify the most efficacious point for potential intervention, we began characterization of the defect progression by first evaluating

TABLE 1
Peak Percentage Weight Loss and Survival (day 21 after Infection) of C57BL/6 Mice Irradiated as Neonates (14 Days Old; Sham Irradiation vs. 5 Gy TBI) and Challenged with Intranasal 1×10^4 EID_{50} of Influenza A/HK/X31 (H3N2 Influenza Virus) or Mock Infection (PBS) at 3, 6 or 9 Months Postirradiation (*9*)

	3 Months		6 Months		9 Months	
Age	Weight loss	Survival after infection	Weight loss	Survival after infection	Weight loss	Survival after infection
Sham irradiation + PBS	5%	100%	4%	100%	5%	100%
5 Gy TBI + PBS	5%	100%	8%	100%	5%	100%
Sham irradiation + influenza	10%	100%	20%	100%	25%	100%
5 Gy TBI + influenza	11%	100%	30%	80%	35%	42%

the immediate impact of neonatal TBI on SLO. Seven days after 5 Gy TBI of 4-day-old mice, mediastinal lymph nodes and spleen were collected and their respective resident cells were enumerated by flow cytometry. This analysis indicated that, as may be anticipated, there was a significant reduction in the number of $CD45^+$ cells ($P = 0.02$), $CD19^+$ B cells ($P = 0.03$), $CD4^+$ T cells ($P = 0.05$) and $CD11c^+$ dendritic cells ($P = 0.02$) (Fig. 1A, D, E and F, respectively) in MLN during this early period postirradiation, although, interestingly, there was an increase in both $CD45^-$ nonhematopoietic cells ($P < 0.0001$) (Fig. 1B) and lineage-$CD3^-CD4^+CXCR5^+$ LTi ($P = 0.01$) (Fig. 1C). Similarly, $CD19^+$ B cells, $CD4^+$ T cells and $CD11c^+$ DC were significantly reduced in the spleens of the irradiated animals, ($P < 0.0001$ for all populations, Fig. 2A–C). Although these data cannot be considered necessarily novel, they provide confirmation of the radiation-sensitive nature of the various cell subpopulations in the neonate model (compared to the adult), as well as the extent of cell loss during a critical developmental period for SLO.

Since stromal cells produce homeostatic chemokines that are important for the recruitment of lymphocytes to SLO, we next determined whether TBI affected expression of stromal cell-related molecules. We found that TBI did not appear to alter expression of CXC chemokine ligand 13 (CXCL13), CC chemokine ligand 19 (CCL19) and fucosyl transferase VII (Fuctvii, an HEV marker; Fig. 3A–C), but saw a significant reduction in expression levels of CD21 ($P = 0.04$), a classic FDC marker also known as complement receptor 2 (Fig. 3D).

To visualize the early systemic effect of TBI on SLO pathology and their spatial cell distribution, we stained frozen sections from anatomically distributed lymph nodes using antibodies specific for both lymphocytes and stromal cells. In various peripheral lymph nodes (MLN, ILN, MeLN) from sham-irradiated mice, large $B220^+$ B-cell

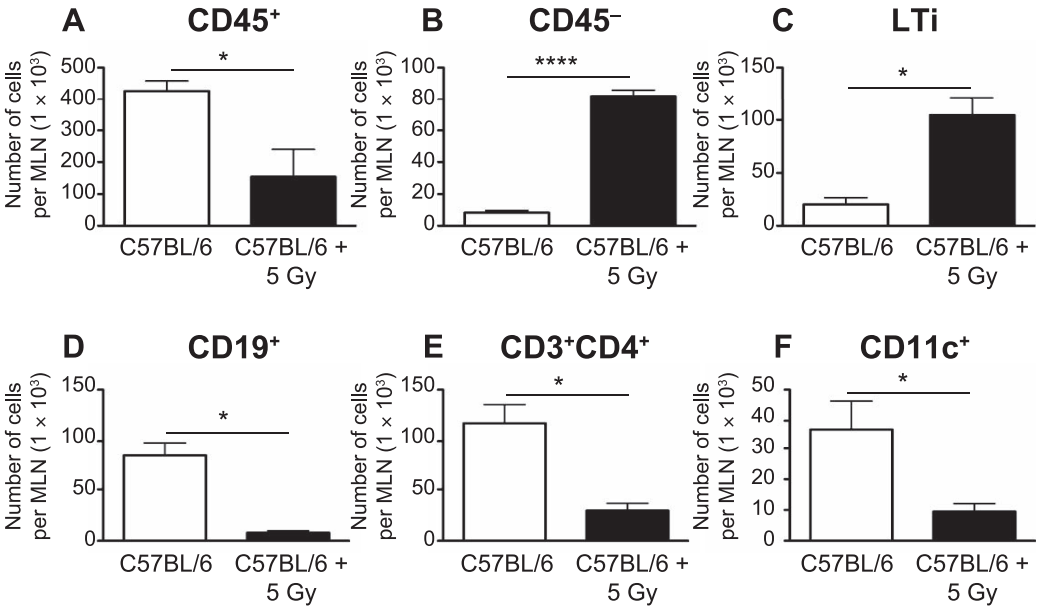

FIG. 1. $CD45^+$ hematopoietic cells (panel A), $CD45^-$ nonhematopoietic cells (panel B) and lymphoid tissue inducer cells [lineage-$CD3^-CD4^+CXCR5^+$(LTi)] (panel C) from the mediastinal lymph nodes (MLN) of sham-irradiated and irradiated neonate mice were counted by flow cytometry at 7 days post irradiation. Total numbers of $CD19^+$ B cells (panel D), $CD3^+CD4^+$ T cells (panel E) and $CD11c^+$ dendritic cells (panel F) are also shown. n = 5 mice/group. Graphs represent mean ± SEM. *$P < 0.05$; ****$P < 0.0001$.

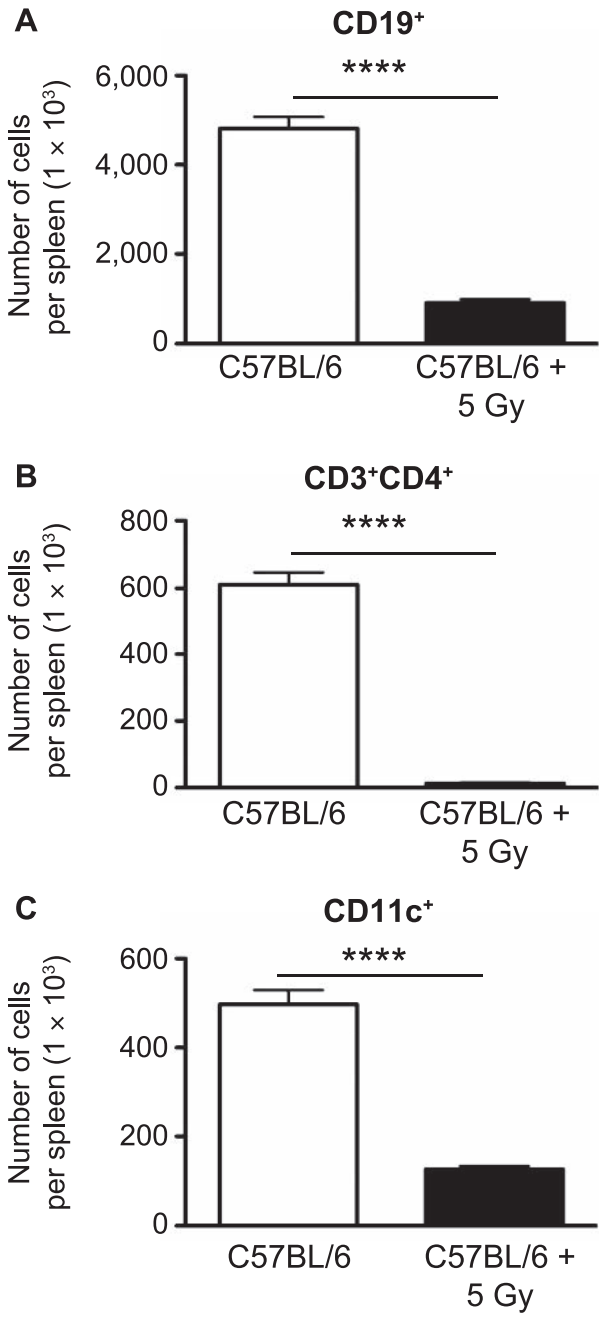

FIG. 2. CD19$^+$ B cells (panel A), CD3$^+$CD4$^+$ T cells (panel B) and CD11c$^+$ dendritic cells (panel C) from spleens of sham-irradiated and irradiated neonate mice were counted by flow cytometry at 7 days after exposure. n = 5 mice/group. Graphs represent mean ± SEM. ****$P < 0.0001$.

follicles with complex and concentric CD21$^-$CD35$^+$ FDC networks were surrounded by CD3$^+$ T cells (Fig. 4A–C) and abundant CD11c$^+$ DC could be identified interacting with large peripheral node addressin$^+$ (PNAd$^+$) HEV (Fig. 5A–C). Spleens from sham-irradiated mice also exhibited well-organized B220$^+$ B-cell follicles containing CD21$^-$CD35$^+$ FDC networks and CD3$^+$ T cells (data not shown). In contrast, the lymph nodes from the previously irradiated animals demonstrated an obvious reduction in the number of B220$^+$ B cells and an apparent complete loss of FDC networks (Fig. 4D–F). The PNAd$^+$ HEV were smaller, whereas the lymphatic vessels appeared to be dilated in the irradiated animals; CD11c$^+$ dendritic cells were less abundant and the contact with HEV was less evident (Fig. 5D–F). Similarly, B220$^+$ B cells, CD3$^+$ T cells and CD11c$^+$ DC were reduced in the spleens after irradiation (data not shown).

Focusing on MLN due to their specific role in thoracic drainage, MLN cellular and structural changes were visualized by bright-field and fluorescent microscopy, and specific changes were confirmed through morphometric analysis, with irradiated animals demonstrating a significant reduction in overall MLN size ($P = 0.03$) relative to the sham-irradiated controls (Fig. 6A). In addition, radiation exposure induced significant decreases in the average size of the B-cell follicles ($P = 0.006$; Fig. 6B) and HEV ($P < 0.0001$; Fig. 6C), as well as the percentage area of the MLN covered by B-cell follicles in MLN from irradiated mice ($P = 0.0226$; Fig. 6D). These results support the hypothesis that the anticipated loss of radiation-sensitive lymphocyte lineage cells after even low (sublethal) doses of TBI impacts not only the cellularity, but SLO structure, in neonate mice during the early time period after irradiation. Furthermore, our findings indicate a systemic effect from radiation exposure on multiple SLO, suggesting that downstream effects on immune function are likely due to a global defect rather than from being linked to alterations in tissue-specific lymphatic drainage.

Delayed Effects of Neonatal Radiation Exposure on Adult SLO: Cytokine, Chemokine and Growth Factor Expression

Previous studies from our group have shown that neonatal radiation exposure is associated with the production of pro-inflammatory molecules that have been implicated in the chronic inflammation and tissue remodeling associated with progression towards late radiation-induced pulmonary effects (*22, 23*). However, some investigators have proposed that these same pro-inflammatory molecules are protective in the context of the response to infection (*24–26*), so may not necessarily play a role in the observed increased susceptibility to influenza. Furthermore, the radiation doses being assessed were far below the putative threshold level associated with the classic end point of either pneumonitis or fibrosis (~12.5 Gy in C57BL/6). Therefore using quantitative PCR, we investigated whether neonatal radiation exposure induced changes in the pulmonary signaling expression of interferon γ (IFN-γ), which plays a critical role in both innate and adaptive immune responses to infection, as well as IFN-γ-induced chemokines [CXC ligand chemokine 9 (CXCL9), CXCL10 and CXCL11]. We assessed the lungs of neonatally irradiated or age-matched sham-irradiated 2-

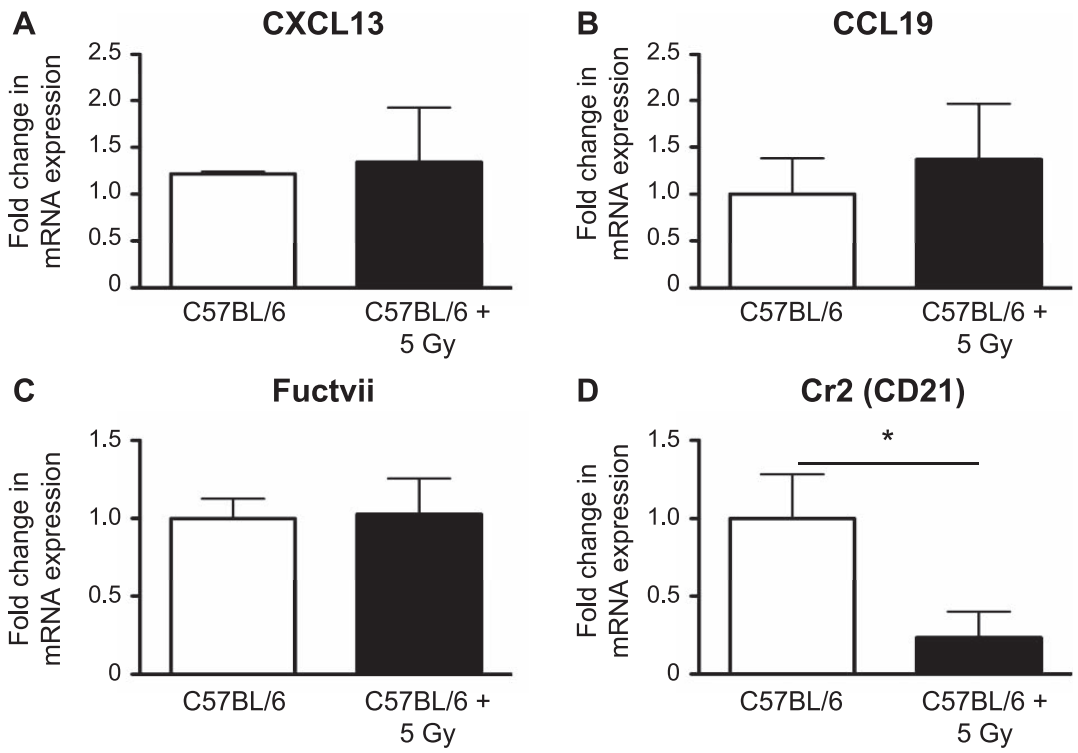

FIG. 3. The stromal cell-related molecules from MLN were assessed 7 days postirradiation by quantitative PCR. mRNA expression was first normalized to GAPDH and mRNA expression levels in the irradiated and sham-irradiated mice were compared. Panel A: CXCL13; panel B: CCL19; panel C: Fuctvii; and panel D: Cr2. n = 5 mice/group. Graphs represent mean ± SEM. *P <0.05.

and 6-month-old mice, time points associated with either baseline or increasing response to infection.

At 2 months postirradiation, significant increases in the expression levels of IFN-γ, CXCL9, CXCL10 and CXCL11 were seen in the lungs of the irradiated mice relative to the age-matched controls (Fig. 7A–D). Since structural changes were already apparent at this stage, this may be part of a compensatory mechanism. Interestingly, although the 6-month-old control mice demonstrated age-related increases in the expression levels of all 4 signals compared to the 2-month-old control animals, the reverse was seen with the irradiated cohort, which demonstrated expression levels closer to the 2-month-old controls and, therefore, had expression levels lower than their age-matched controls. It is worth noting that although significant increases in the expression levels of collagen type I and fibronectin were observed in the 2-month-old animals (Fig. 7E and F), levels had returned to baseline by 6 months, a time point typically associated with radiation-induced pulmonary fibrosis, confirming that the doses used were, indeed, below the threshold level for fibrosis induction.

PCR was also performed with respect to expression levels in MLN, assessing chemokines and molecules that are important in directing lymphocyte trafficking, such as CXCL13 (a B-cell chemoattractant) and CCL19 (a T- and B-cell chemoattractant), as well as complement receptor 2/CD21 and fucosyltransferase VII (Fuctvii). Similar to the analysis in lung, we saw an age-related increase in all 4 signals in the MLN between the 2- and 6-month-old control animals, as well as significant increases in expression in the irradiated 2-month-old mice (Fig. 8A–D). Of note, CXCL13 expression was also increased in the lungs of irradiated 2-month-old mice (data not shown). Interestingly, the age-dependent increase in CD21 and Fuctvii expression levels appeared to be further enhanced by the neonatal radiation exposure (Fig. 8C and D).

These results support our previous findings (*9*), which had demonstrated that in the first few months after neonatal irradiation, animals are capable of responding normally to the influenza infection. This response is likely due to the increased expression of homeostatic chemokines in MLN and IFN-γ-induced chemokines in the lungs, accelerating the initiation of adaptive immunity in draining lymph nodes, attracting $CXCR3^+$ and $CXCR5^+$ effector lymphocytes to the infected lungs, and thus facilitating the elimination of influenza viruses and the resolution of the pulmonary infection. However, by later time points (≥6 months postirradiation), the decrease in chemokine expression levels relative to age-matched controls supports the observation of an exacerbated response to infection due to the lung and MLN's inability to effectively initiate adaptive immunity.

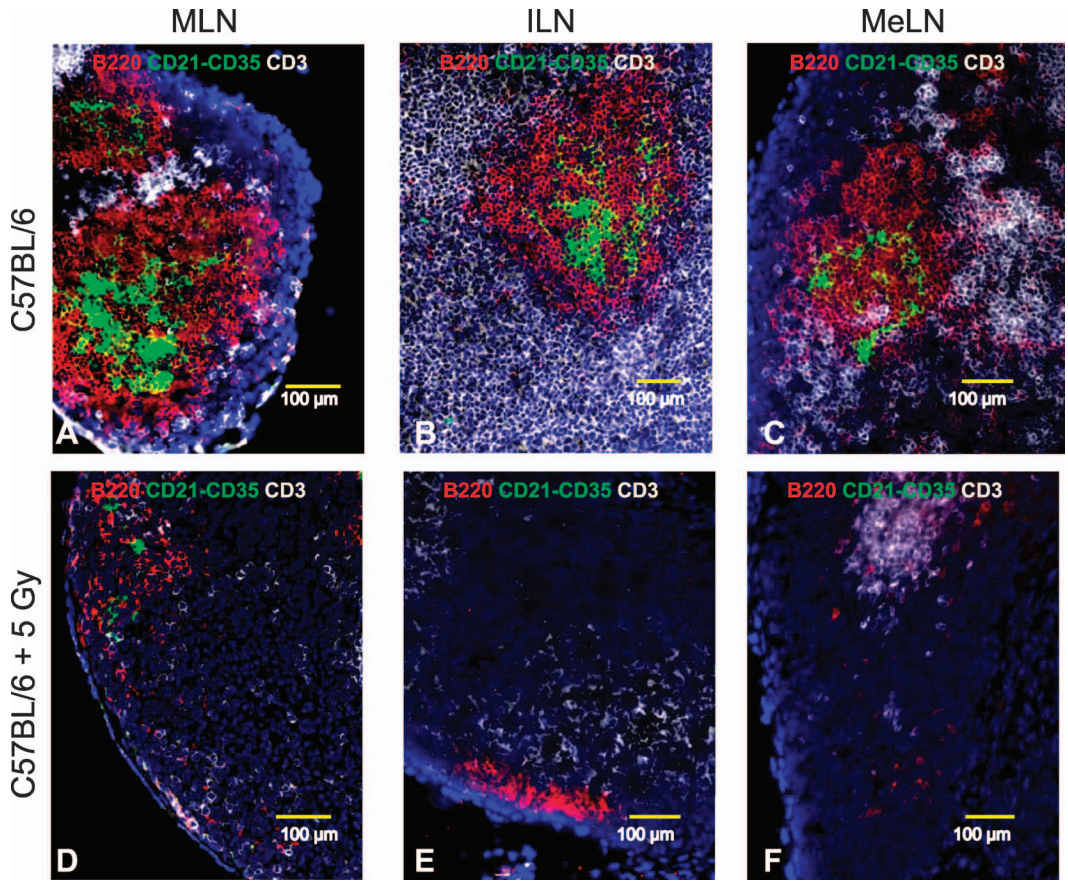

FIG. 4. SLO cell composition was assessed in neonate mice 7 days postirradiation (frozen sections stained with fluorescent antibodies). Representative 200× pictures for $B220^+$ B-cell follicles (red), $CD21^-CD35^+$ FDC networks (green) and T cell areas (white) in mediastinal lymph nodes [MLN; panel A (sham irradiated) and panel D (5 Gy TBI)], inguinal lymph nodes [ILN; panel B (sham irradiated) and panel E (5 Gy TBI)] and mesenteric lymph nodes [MeLN: panel C (sham irradiated); panel F (5 Gy TBI)] are shown.

Delayed Effects of Neonatal Radiation Exposure on Adult Lung Response to Influenza

To directly determine whether alterations in neonatal SLO induced by TBI affected the outcome from influenza infection, as previously observed, we measured the expression of influenza acid polymerase (PA), evaluated influenza-associated morbidity and enumerated influenza-nucleoprotein (NP) specific T cells by flow cytometry in the lungs of animals infected at 2 and 6 months after irradiation. PA expression has been previously used as an indicator of the control of influenza infection (*27, 28*). In contrast to our earlier studies (*9*), the neonatally irradiated 2-month-old mice demonstrated a delayed viral clearance (increased PA expression, $P = 0.03$; Fig. 9A). Nonetheless, in all other aspects, progression of the infection matched that seen in the age-matched controls, as assessed by changes in body weight (Fig. 9B) and a normal accumulation of pulmonary $CD3^+CD8^+NP^+$ and $CD3^+CD4^+NP^+$ T cells (Fig. 9C and D). The previously irradiated 6-month-old mice exhibited a similar viral load to the age-matched controls and recovered normally from infection (Fig. 10A and B). However, in contrast to the response seen in the 2-month-old mice, $CD3^+CD8^+NP^+$ ($P = 0.04$) and $CD3^+CD4^+NP^+$ T cells ($P = 0.002$) were significantly reduced in the previously irradiated animals at the peak of the immune response against the influenza virus on day 10 after infection (Fig. 10C and D) supporting the hypothesis that neonatal radiation exposure had induced a progressive pulmonary compromise.

Delayed Effects of Neonatal Radiation Exposure on Adult MLN Response to Influenza

Although neonatal TBI did not appear to have affected the overall level of protection against influenza in the irradiated 2-month-old mice, we evaluated the functional induction of adaptive immunity in MLN. Although the numbers of $CD3^+CD8^+NP^+$ T cells were decreased in the irradiated animals relative to age-matched controls, this did not reach the level of significance (Fig. 11A); however, there was a significant reduction in the numbers of $CD3^+CD4^+NP^+$ T cells ($P = 0.0031$; Fig. 11B), Treg ($Foxp3^+$; $P = 0.002$; Fig. 11C) and TFH ($P = 0.0001$; Fig. 11D) on day 10 after infection in MLN from irradiated 2-month-old mice, the peak day of response in the control animals. Nonetheless,

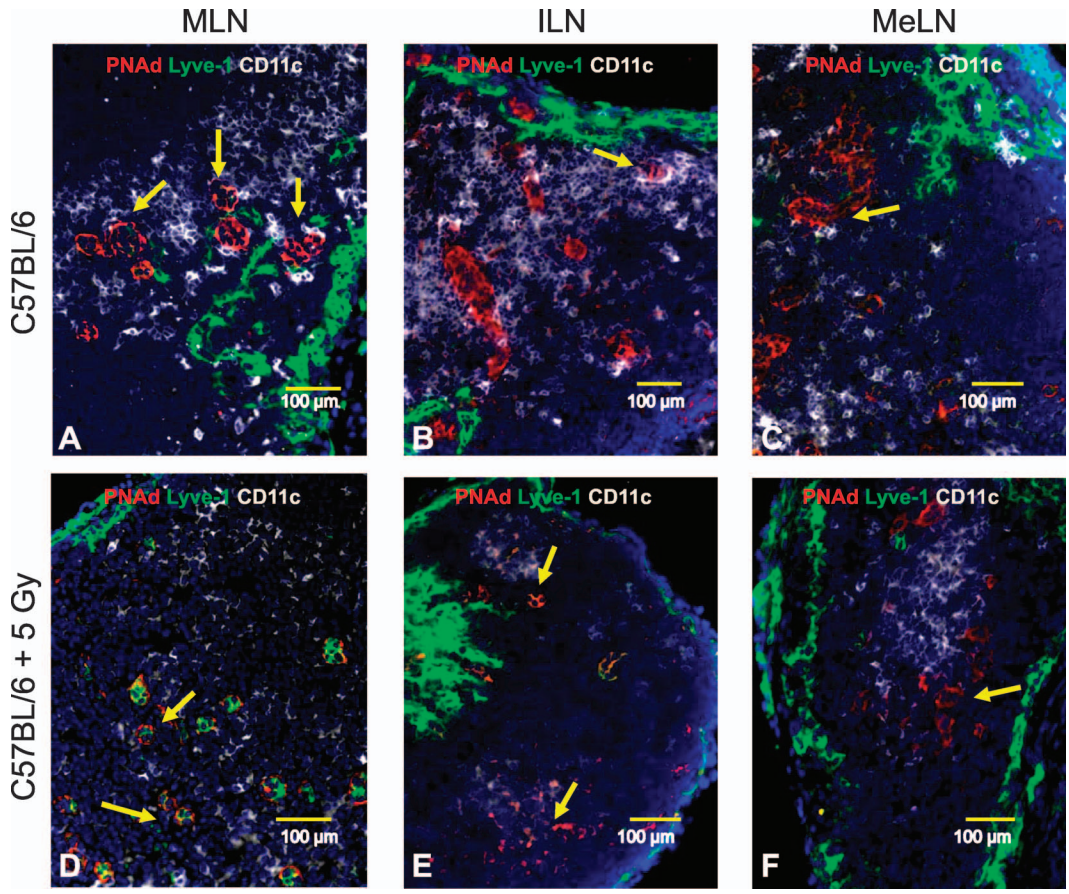

FIG. 5. SLO structure was assessed in neonate mice 7 days postirradiation (frozen sections stained with fluorescent antibodies). Representative 200× pictures for PNAd$^+$ HEV (red), Lyve-1$^+$ lymphatics (green) and CD11c$^+$ dendritic cells (white) in mediastinal lymph nodes [MLN; panel A (sham irradiated) and panel D (5 Gy TBI)], inguinal lymph nodes [ILN; panel B (sham irradiated) and panel E (5 Gy TBI)] and mesenteric lymph nodes [MeLN; panel C (sham irradiated) and panel F (5 Gy TBI)] are shown. Yellow arrows identify PNAd$^+$ HEV.

despite the simultaneous significant reductions in TFH and influenza-specific IgG antibodies ($P = 0.01$; Fig. 11D and F), the production of germinal center B cells (CD19$^+$CD95$^+$PNA$^+$) did not appear to have been affected by the earlier irradiation (Fig. 11E). Interestingly, we did not find any differences in the generation of NP$^+$ T cells, TFH, Treg or GCB in MLN among infected 6-month-old irradiated and age-matched control animals (data not shown).

Finally, to determine whether the early structural changes seen in HEV and B-cell follicles of neonatally irradiated mice were still evident in adult life, we assessed the dimensions of HEV before and after challenge with influenza virus. HEV were significantly smaller in MLN from irradiated 2-month-old mice relative to controls both before and after infection (Fig. 12A). In addition, we detected a significant reduction in the size of the germinal centers in spleens of irradiated mice relative to controls (assessed on day 14 after infection) whether infected at 2 or 6 months of age (Fig. 12B).

DISCUSSION

We believe that the results from this study provide unique evidence that neonatal TBI not only has an early effect on the cellular composition and structure of SLO, but is also associated with a long-term and progressive detrimental impact on the induction of B-cell and CD4$^+$ T-cell responses in the SLO of adult mice, which affect the animals' ability to respond to an infection challenge from the influenza virus. For example, we demonstrate the loss of dendritic cells early postirradiation; these hematopoietic cells are critical for the generation and differentiation of antigen-specific T cells, including TFH, that participate actively in the germinal center reaction against foreign pathogens (*29*). In addition, recent evidence indicates that DC are essential for the formation and growth of HEV (*15, 30*), which are the portals for entry of naïve T cells into SLO. B cells also are important in the generation of FDC and for vascular cell growth in immune-reactive lymph nodes (*10, 31–33*). Therefore, the early damage inflicted by radiation exposure on the neonatal DC and B-cell

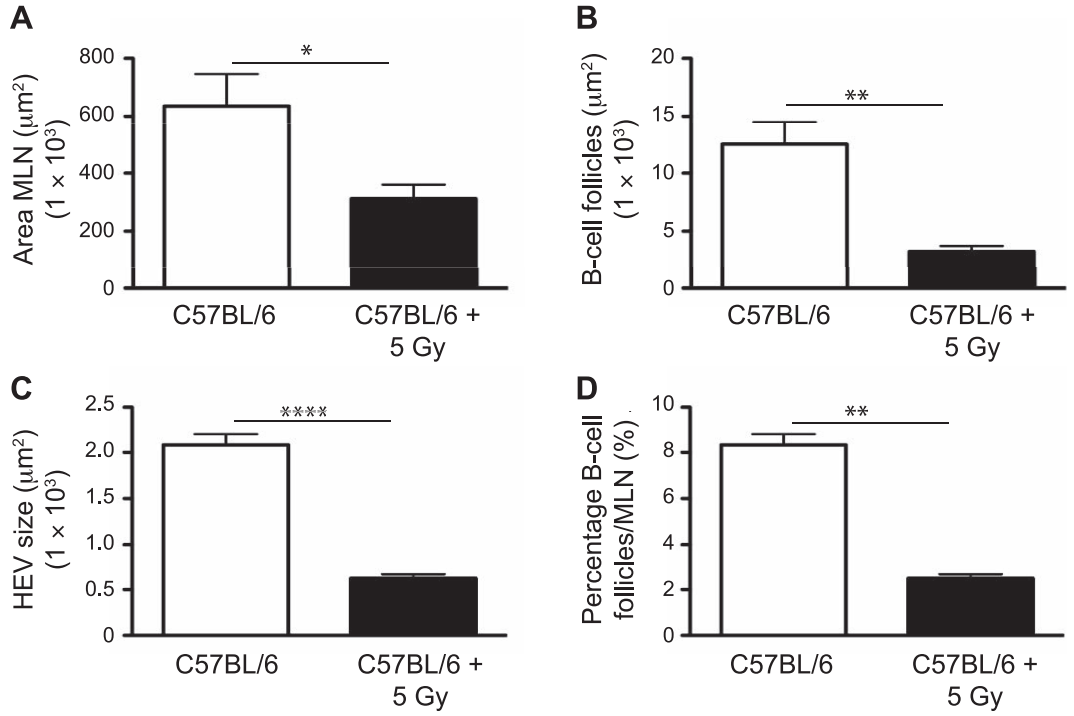

FIG. 6. Morphometric analyses of structural and cellular changes in MLN performed at 7 days postirradiation were determined using an automated tool from Zeiss AxioVision software. Panel A: Dimensions of MLN; panel B: average size of B-cell follicles; panel C: HEV; and panel D: percentage covered by B-cell follicles/MLN section. n = 5 mice per group. Graphs represent mean ± SEM. *$P < 0.05$; **$P < 0.005$; ****$P < 0.0001$.

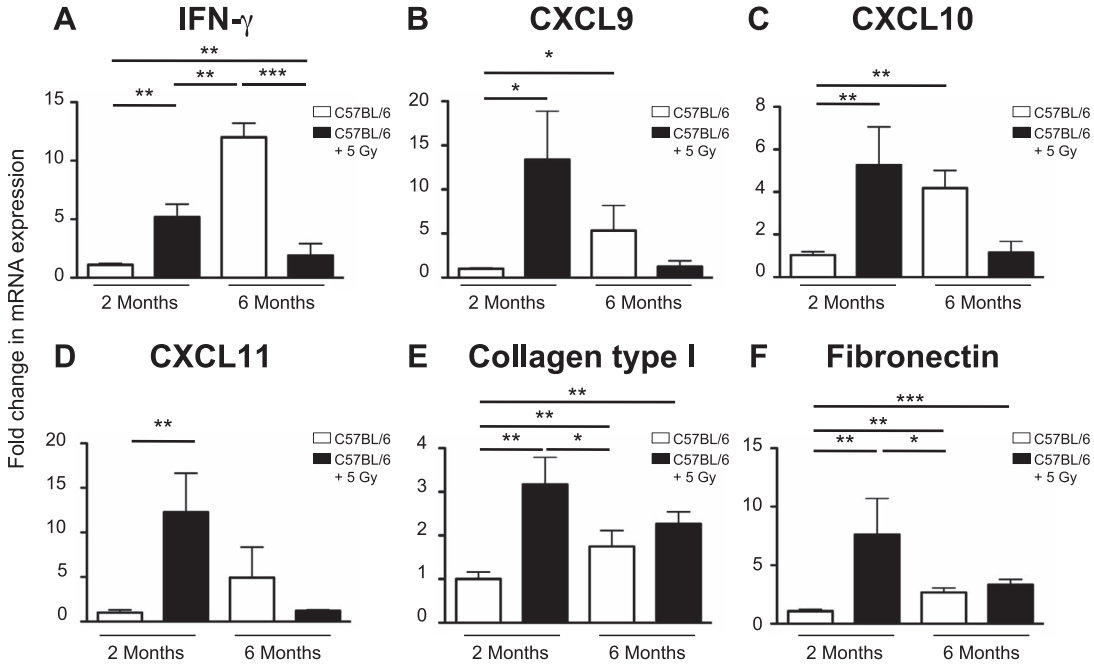

FIG. 7. Pulmonary expression levels of IFN-γ and IFN-γ-induced chemokines were determined by quantitative PCR in lungs from nonirradiated (age-matched) or neonatally irradiated mice at 2 and 6 months postirradiation. mRNA expression was first normalized to GAPDH and mRNA expression levels in irradiated groups were compared to mRNA levels in sham-irradiated 2-month-old mice. Panel A: IFN-γ; panel B: CXCL9; panel C: CXCL10; panel D: CXCL11; panel E: collagen type I; and panel F: fibronectin. n = 5/group. Graphs represent mean ± SEM. *$P < 0.05$; **$P < 0.005$; ***$P < 0.0005$.

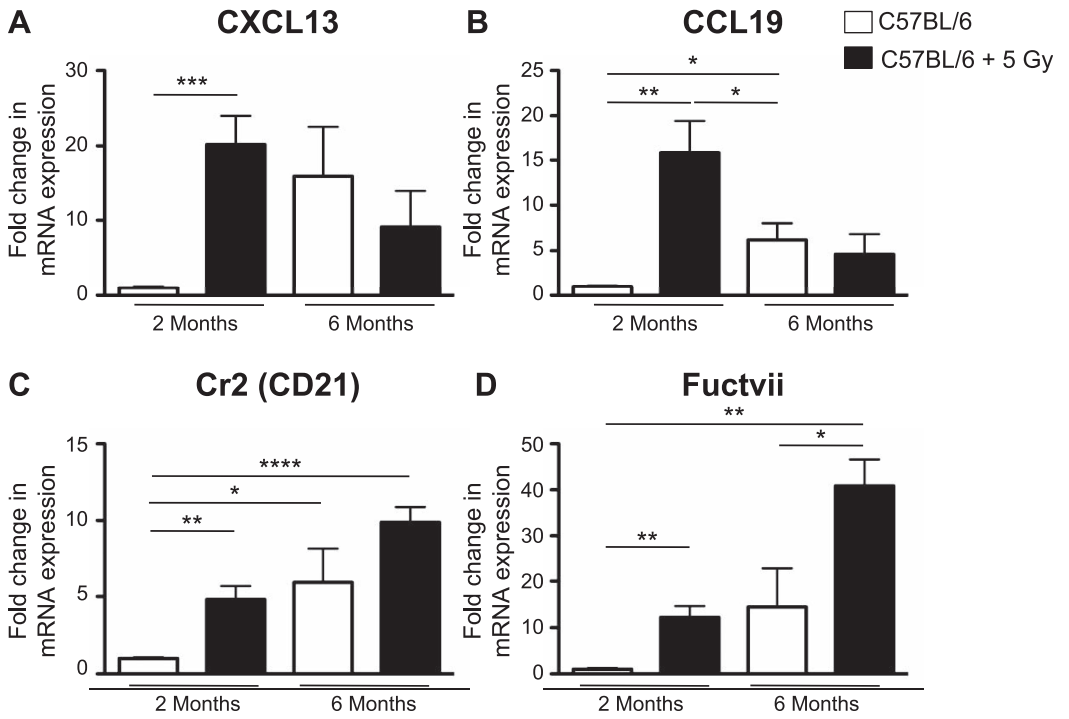

FIG. 8. Expression levels of signals associated with lymphocyte trafficking were determined by quantitative PCR in MLN from nonirradiated (age-matched) or neonatally irradiated mice at 2 and 6 months postirradiation. mRNA expression was first normalized to GAPDH and mRNA expression levels in the irradiated group were compared to mRNA levels in sham-irradiated 2-month-old mice. Panel A: CXCL13; panel B: CCL19; panel C: Cr2; and panel D: Fuctvii. n = 5/group. Graphs represent mean ± SEM. *$P < 0.05$; **$P < 0.005$; ***$P < 0.0005$; ****$P < 0.0001$.

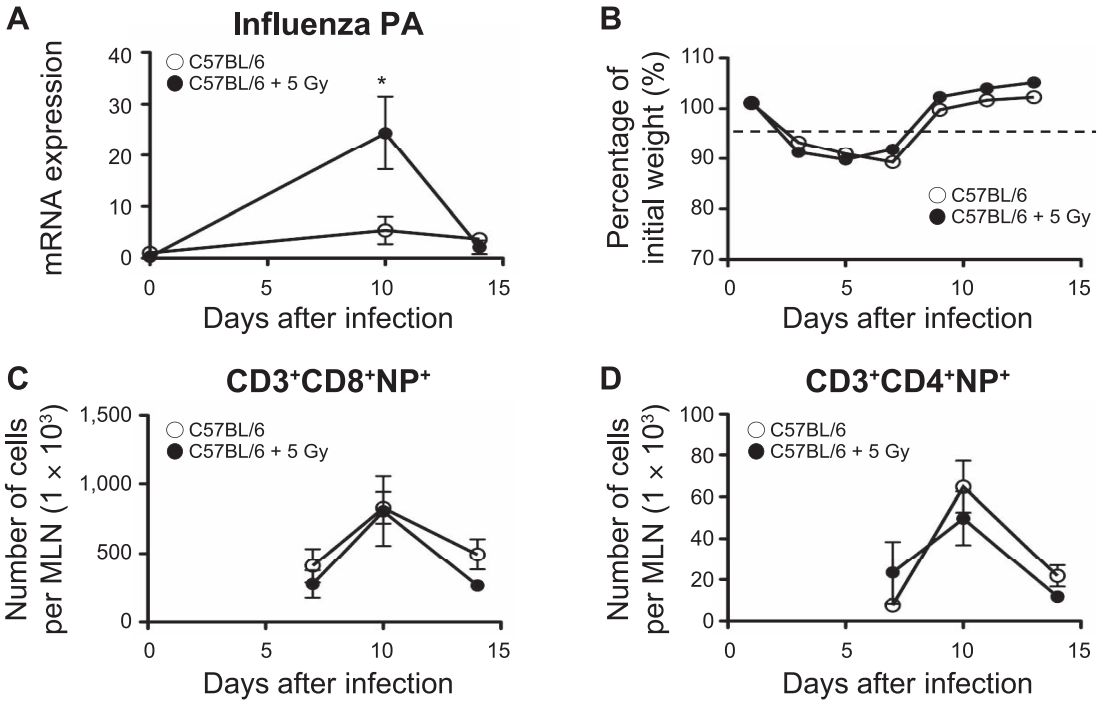

FIG. 9. The effect of influenza infection in lungs of 2-month-old mice. Panel A: Changes in influenza PA expression determined by quantitative PCR. Panel B: Changes in body weight monitored every other day during influenza infection. Panels C and D: Kinetics of accumulation of effector lymphocyte T cells [$CD3^+CD8^+NP^+$ T cells (panel C) and $CD3^+CD4^+NP^+$ T cells (panel D)], assessed in lungs of sham-irradiated and neonatally irradiated mice by flow cytometry. n = 5/group. Graphs represent mean ± SEM. *$P < 0.05$.

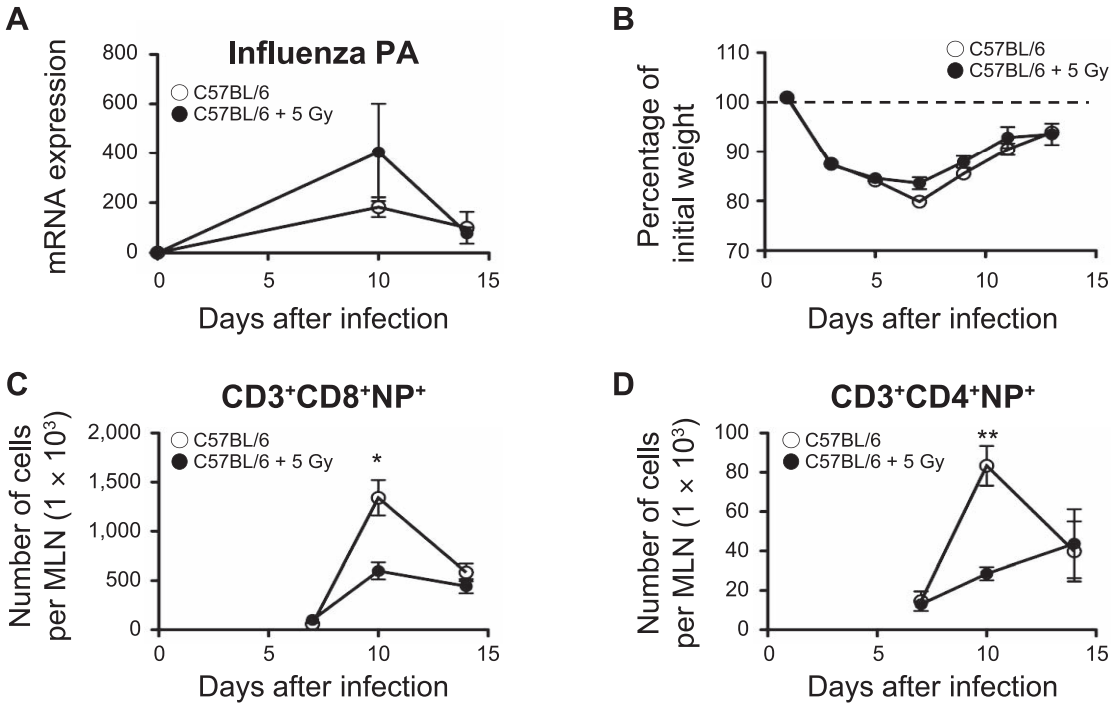

FIG. 10. The effect of influenza infection in lungs of 6-month-old mice. Panel A: Changes in influenza PA expression determined by quantitative PCR. Panel B: Changes in body weight monitored every other day during influenza infection. Panels C and D: Kinetics of accumulation of effector lymphocyte T cells [$CD3^+CD8^+NP^+$ T cells (panel C) and $CD3^+CD4^+NP^+$ T cells (panel D)], assessed in lungs of sham-irradiated and neonatally irradiated mice by flow cytometry. n = 5/group. Graphs represent mean ± SEM. $^*P < 0.05$; $^{**}P < 0.005$.

populations, indicated by the presence of relatively small HEV and the absence of FDC in the irradiated neonatal SLO, suggests the potential for such an injury to affect the long-term DC capacity to induce the generation/expansion of HEV and to prime T cells. Chronic structural and functional alterations would be reflected in impaired recruitment and priming of naïve T cells in SLO and, indeed, long-term dysfunction of both DC and B-cell populations was evidenced by an impairment in $CD4^+$ T-cell priming, TFH differentiation and GC formation in the SLO of the adult mice after neonatal irradiation (Figs. 9–11).

Much of the early (day 7 postirradiation) results shown should not be considered novel or surprising given the broad acceptance that bone marrow-derived cell populations, in particular B cells, are highly radiation sensitive, even after relatively low sublethal doses (*34, 35*). Therefore, the demonstration of a significant early loss of neonatal B cells and the absence of FDC in the spleens of mice exposed to TBI is consistent with this dogma. However, since FDC are the main source of CXCL13 in SLO (*36*), we were somewhat surprised to detect CXCL13 expression in MLN from irradiated neonate mice that apparently lacked $CD21^-CD35^+$ FDC. It is therefore likely that, in the immediate absence of FDC, surviving LTi may be stimulating CXCL13 expression through the slower responding, putatively more radioresistant, $CD45^-$ stromal cells, which were observed as having increased in number after irradiation (Fig. 1B). Interestingly, we found that TBI caused a pronounced, but differential, reduction in neonatal $CD4^+$ T cells, with a 50-fold reduction in the spleen compared to a more moderate reduction (fourfold) observed in MLN (Fig. 1E compared to Fig. 2B). This finding suggests that local niches and cell–cell interactions in different SLO may affect the radiation outcome of resident cells and, as a result, influence the downstream fate of stromal cell populations. For example, the depletion of neonatal B cells from the spleens of irradiated neonate mice was associated with the apparent complete loss of FDC in that organ at 7 days postirradiation (Fig. 4D–F). In addition, the significant depletion of lymphocytes from both neonatal spleen and MLN suggests that perhaps both hematopoiesis and recruitment of lymphocytes were affected in SLO (*37*). In contrast, the presence of surviving $LT\alpha_1\beta_2$-expressing DC in the MLN of irradiated mice over the same time period (data not shown) resulted in structural changes in the HEV, but not their elimination, suggesting some degree of niche protection.

With respect to the potentially chronic changes that may affect the downstream response to infection, NP-specific $CD8^+$ T cells play a dominant role in protection against influenza viruses during primary infection (*38*). Although the accumulation of $CD8^+NP^+$ T cells in the infected lungs of mice at 2 months postirradiation appeared to be at normal levels (Fig. 9), we nonetheless demonstrated that $CD4^+$ T cell priming and generation of TFH and Treg were impaired

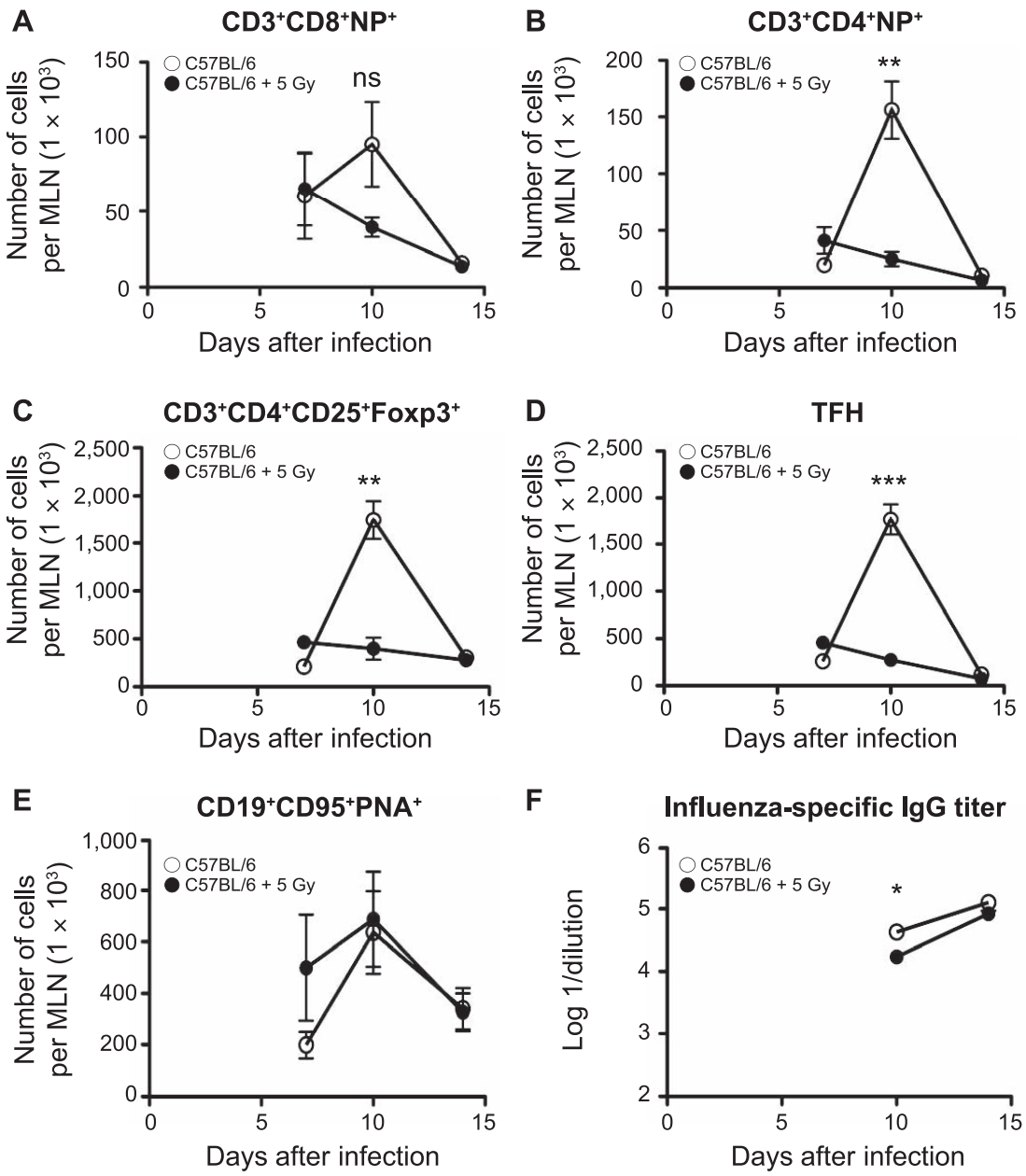

FIG. 11. Populations of effector lymphocytes from MLN of infected control or neonatally irradiated animals were counted by flow cytometry at 2 months postirradiation. Panel A: $CD3^+CD8^+NP^+$ T cells; panel B: $CD3^+CD4^+NP^+$ T cells; panel C: $CD3^+CD4^+CD25^+Foxp3^+$ Treg; panel D: TFH; panel E: germinal center B cells ($CD19^+CD95^+PNA^+$). Serum was collected at different time points and influenza-specific IgG titer was determined by ELISA (panel F). Data show the logarithm of reciprocal dilution at which the optical density was equal to 0.2. n = 5/group. Graphs represent mean ± SEM. $*P < 0.05$; $**P < 0.005$; $***P < 0.0005$.

in MLN at that same time (Fig. 11B–D). Since previous studies have suggested that radiation affects the capacity of DC to prime T cells (*34*), the observed defective $CD4^+$ T-cell priming and TFH differentiation in our mouse model may be associated with the presence of dysfunctional DC at 2 months postirradiation. Although we did not directly determine functionality of DC at the later time points, other investigators have shown that gamma radiation impairs DC migration toward CCL19 produced in SLO (*31*), a finding that is consistent with our early observations of a significant reduction in $CD11c^+$ DC in MLN of irradiated neonate mice. Since DC are critical in HEV differentiation and expansion, it is likely that the observed structural changes in HEV seen in systemically distributed lymph nodes of neonatally irradiated mice (Fig. 5D–F) may contribute to poor recruitment of naïve T cells, indirectly having a negative impact on $CD4^+$ T-cell priming.

Although TFH numbers were reduced in MLN of 2-month-old mice exposed to TBI as neonates, we detected similar numbers of GCB cells compared to age-matched

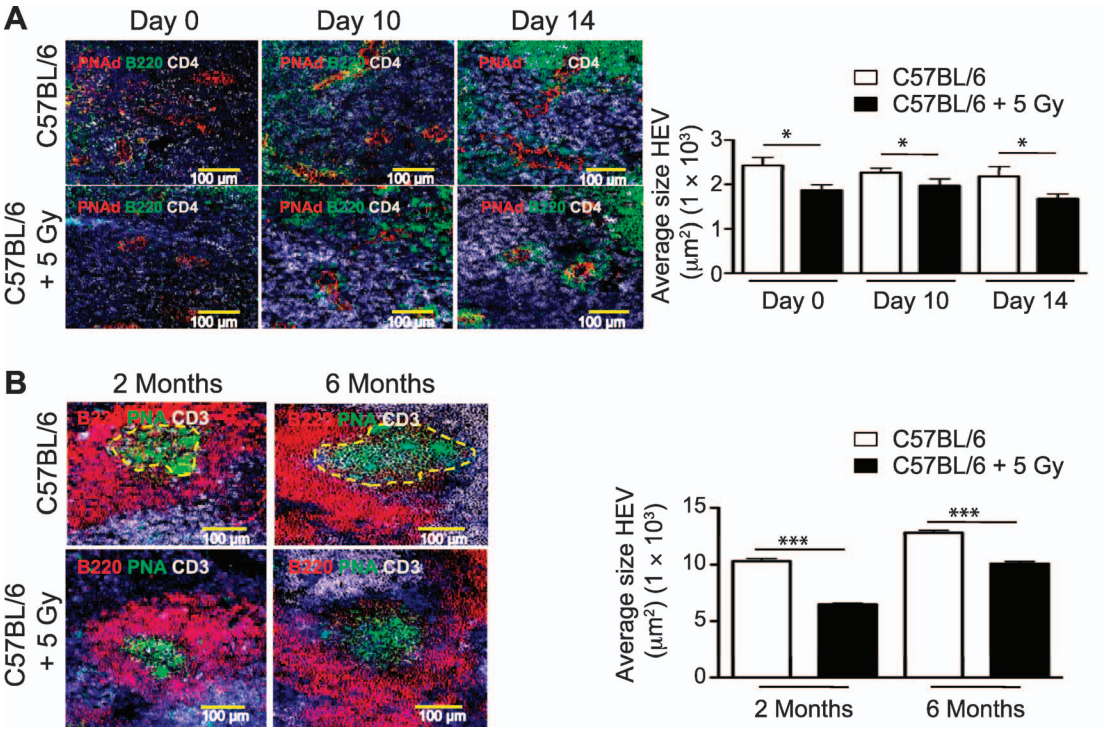

FIG. 12. Morphometric analyses of structural and cellular changes in MLN and spleens were performed at 2 and 6 months postirradiation. Panel A: Representative 200× pictures of PNAd$^+$ HEV (red vessels), B220$^+$ B cells (green cells) and CD4$^+$ T cells (white cells) in MLN from control and neonatally irradiated 2-month-old mice before infection (day 0) or after influenza challenge (day 10 and 14 after infection). Panel B: Spleen frozen sections from influenza-infected, sham-irradiated and irradiated C57BL/6 mice (2 and 6 months of age) were stained with antibodies against B220 (red), CD3 (white) and peanut agluttinin (green) to detect PNA$^+$ germinal centers. PNA$^+$ GC were measured using an automated tool from the Zeiss Axioplan software and the average size of GC was calculated. Representative 200× pictures of peanut agglutinin-binding GC are outlined with dashed yellow lines (day 14 after infection). HEV dimensions and GC size were determined using an automated tool from the Zeiss AxioVision software. n = 5/group. Results represent mean ± SEM. $*P < 0.05$; $***P < 0.005$.

controls. Recently, it has been shown that TFH are able to migrate to multiple GC to support B-cell differentiation and antibody production (*32*), thus, it is likely that the surviving TFH seen in MLN of irradiated 2-month-old mice were sufficient to induce differentiation of naïve B cells into GCB. For comparison purposes, human Tregs have also been shown to be sensitive to low doses of radiation (*39*) and migrate inside GC (*40*). Thus, based on the reduction of Tregs seen in MLN from irradiated 2-month-old mice during influenza infection, we might expect that modulation of the GC response by Tregs will be compromised in these mice. In addition, increased production of CXCL13 in the MLN of the irradiated animals will promote competition between niches in the GC among CXCR5-expressing cells (*13, 41*), compromising TFH differentiation. Nevertheless, the current results suggest that the number of surviving TFH was sufficient to support the induction of normal humoral responses against influenza viruses, at least at the 2- and 6-month time points after irradiation. However, our earlier data indicate that this may not be true in the long term (≥9 months postirradiation; Table 1) (*9*).

Importantly, neonatal TBI had a chronic and detrimental impact on GC formation in the spleens of mice challenged with influenza virus at 2 and 6 months postirradiation (Fig. 12B). As a result of the significant reduction in splenic CD4$^+$ T cells seen after neonatal TBI, it is likely that repopulation led to intrinsic defects in CD4$^+$ T cells associated with defective TFH differentiation, affecting GC responses in the adult spleen and impairing the production of high-affinity antibodies. Interestingly, it is the CD8$^+$ T cells that play a dominant role in the induction of protective immunity during a primary influenza infection (*42*), providing an explanation for the infection control seen in the previously irradiated mice. Therefore, we hypothesize that neonatal radiation exposure will affect the induction of protective humoral immunity after infections from extracellular pathogens and will be seen in experimental systems that allow the measurement of antibody affinity.

With respect to radiation-induced changes in cell signaling, IFN-γ-induced chemokines have been shown to play a key role in the defense of the respiratory tract (*24–26*) so that their early increased expression levels (Fig. 7), together with the enhanced expression of homeostatic

chemokines (CCL19, CXCL13) in MLN (Fig. 8) of neonatally irradiated mice also likely contributed at first to recovery from influenza infection in adult life; the increased expression above that of the age-matched controls likely represents a compensatory mechanism, as suggested earlier. This is consistent with previous studies showing the relevance of CXCL13 and IFN-γ-induced chemokines in the rapid attraction of $CXCR5^+$ and $CXCR3^+$ effector lymphocytes to infected lungs, accelerating pathogen clearance and minimizing lung pathology (*25, 26*). Interestingly, the increased expression levels of fibronectin and collagen I seen in the lungs from irradiated 2-month-old mice (Fig. 7) suggest a possible early initiation of fibrosis (*43*). This time lapse is consistent with the period of time (8 weeks after TBI) required for the induction of small patches of fibrosis in lungs of C57L/J mice exposed to a single dose of thoracic radiation (*44*), but is much quicker than the normal rate of progression seen in C57BL/6 mice (*45*) and was induced at dose levels well below the putative thresholds for pulmonary late effects in either of these strains. The return to baseline expression levels in the irradiated 6-month-old mice confirms the lack of progression to lung fibrosis, however, it is currently unclear what role, if any, these characteristic profibrotic signals may play in the impairment of pulmonary immunity in neonatally irradiated mice. What may be of interest is the potential for their involvement in accelerated radiation-induced senescence, a subject of increasing interest due to its possible role in both tumor and normal tissue response to radiation (*46*). Furthermore, above and beyond their role in mechanism, the altered profiles and temporal expression patterns of these signals may find utility as indicators (biomarkers) of ongoing dysfunction and indicate preferential time points for mitigation or, in this case, perhaps the need for additional vaccination strategies.

To the best of our knowledge, we are the first to provide evidence of the detrimental impact of exposure to gamma radiation on the structure and function of SLO, contrasting with the vast literature in the radiation field that has been focused on the study of the hematopoietic cell compartment in the peripheral blood. Overall, our results reveal the potential for unexpected subclinical impairment in $CD4^+$ T-cell priming, TFH differentiation and GC formation in SLO from mice exposed to sublethal TBI during the neonatal period, leading to a progressive inability to adequately respond to an influenza infection. However, more studies will be required to determine if this increased susceptibility extends to other respiratory and even non-pulmonary extracellular pathogens in young mice exposed to sublethal radiation, as well as the impact of TBI on the induction of protective humoral immunity against pulmonary pathogens that are eliminated by antibodies. From a clinical perspective, our data suggest that TBI of pediatric BMT patients may induce permanent damage in SLO, increasing their susceptibility to pulmonary infections whose clearance depends on antibody production and an intact spleen function. Our results encourage close monitoring of immune function in survivors of childhood BMT to define early treatment windows for appropriate immune intervention.

ACKNOWLEDGMENTS

This work was supported by the Centers for Medical Countermeasures against Radiation Program, NIH/NIAID U19 grant no. AI091036. In addition, JRM was supported by startup funds from the Department of Medicine, University of Rochester, as well as pilot funding from the University of Rochester Center for Medical Countermeasures against Radiation (AI91036).

Received: February 7, 2015; accepted: August 6, 2015; published online: September 23, 2015

REFERENCES

1. Boulad F, Sands S, Sklar C. Late complications after bone marrow transplantation in children and adolescents. Curr Prob Pediatr 1998; 28:273–97.
2. Johnston BL, Conly JM. Immunization for bone marrow transplant recipients. Can J Infect Dis 2002; 13:353–7.
3. Bhatia S, Davies SM, Scott Baker K, Pulsipher MA, Hansen JA. NCI, NHLBI first international consensus conference on late effects after pediatric hematopoietic cell transplantation: etiology and pathogenesis of late effects after HCT performed in childhood - methodologic challenges. Biol Blood Marrow Transplant 2011; 17:1428–35.
4. Chima RS, Abulebda K, Jodele S. Advances in critical care of the pediatric hematopoietic stem cell transplant patient. Pediatr Clin N Amer 2013; 60:689–707.
5. Fazekas T, Attarbaschi A, Lawitschka A, Seidel M, Potschger U, Peters C, et al. Lethal pulmonary complications after pediatric allogeneic hematopoietic stem cell transplantation. Pediatr Infect Dis J 2012; 31:115–9.
6. Holbro A, Lehmann T, Girsberger S, Stern M, Gambazzi F, Lardinois D, et al. Lung histology predicts outcome of bronchiolitis obliterans syndrome after hematopoietic stem cell transplantation. Biol Blood Marrow Transplant 2013; 19:973–80.
7. Kim YJ, Guthrie KA, Waghmare A, Walsh EE, Falsey AR, Kuypers J, et al. Respiratory syncytial virus in hematopoietic cell transplant recipients: factors determining progression to lower respiratory tract disease. J Infect Dis 2014; 209:1195–204.
8. Shelburne N, Bevans M. Non-myeloablative allogeneic hematopoietic stem cell transplantation. Semin Oncol Nurs 2009; 25:120–8.
9. Johnston CJ, Manning CM, Rangel-Moreno J, Randall TD, Hernady E, Finkelstein JN, et al. Neonatal irradiation sensitizes mice to delayed pulmonary challenge. Radiat Res 2013; 179:475–84.
10. Carragher DM, Rangel-Moreno J, Randall TD. Ectopic lymphoid tissues and local immunity. Semin Immunol 2008; 20:26–42.
11. Randall TD, Carragher DM, Rangel-Moreno J. Development of secondary lymphoid organs. Ann Rev Immunol 2008; 26:627–50.
12. van de Pavert SA, Ferreira M, Domingues RG, Ribeiro H, Molenaar R, Moreira-Santos L, et al. Maternal retinoids control type 3 innate lymphoid cells and set the offspring immunity. Nature 2014; 508:123–7.
13. Coles MC, Veiga-Fernandez H, Foster KE, Norton T, Pagakis SN, Seddon B, et al. Role of T and NK cells and IL7/IL7r interactions during neonatal maturation of lymph nodes. Proc Natl Acad Sci U S A 2006; 103:13457–62.
14. Endres R, Alimzhanov MB, Plitz T, Futterer A, Kosco-Vilbois MH, Nedospasov SA, et al. Mature follicular dendritic cell

networks depend on expression of lymphotoxin beta receptor by radioresistant stromal cells and of lymphotoxin beta and tumor necrosis factor by B cells. J Exp Med 1999; 189:159–68.

15. Moussion C, Girard JP. Dendritic cells control lymphocyte entry to lymph nodes through high endothelial venules. Nature 2011; 479:542–6.
16. Tan JK, Watanabe T. Artificial engineering of secondary lymphoid organs. Adv Immunol 2010; 105:131–57.
17. Cremasco V, Woodruff MC, Onder L, Cupovic J, Nieves-Bonilla JM, Schildberg FA, et al. B cell homeostasis and follicle confines are governed by fibroblastic reticular cells. Nat Immunol 2014; 10:973–81.
18. Onder L, Narang P, Scandella E, Chai Q, Iolyeva M, Hoorweg K, et al. IL-7-producing stromal cells are critical for lymph node remodeling. Blood 2012; 120:4675–83.
19. Moltedo B, Lopez CB, Pazos M, Becker MI, Hermesh T, Moran TM. Cutting edge: stealth influenza virus replication precedes the initiation of adaptive immunity. J Immunol 2009; 183:3569–73.
20. Rangel-Moreno J, Carragher DM, de la Luz Garcia-Hernandez M, Hwang JY, Kusser K, Hartson L, et al. The development of inducible bronchus-associated lymphoid tissue depends on IL-17. Nat Immunol 2011; 12:639–46.
21. Rangel-Moreno J, Carragher DM, Misra RS, Kusser K, Hartson L, Moquin A, et al. B cells promote resistance to heterosubtypic strains of influenza via multiple mechanisms. J Immunol 2008; 180:454–63.
22. Johnston CJ, Hernady E, Reed C, Thurston SW, Finkelstein JN, Williams JP. Early alterations in cytokine expression in adult compared to developing lung in mice after radiation exposure. Radiat Res 2010; 173:522–35.
23. Johnston CJ, Manning C, Hernady E, Reed C, Thurston SW, Finkelstein JN, et al. Effect of total body irradiation on late lung effects: hidden dangers. Int J Radiat Biol 2011; 87:902–13.
24. Khader SA, Rangel-Moreno J, Fountain JJ, Martino CA, Reiley WW, Pearl JE, et al. In a murine tuberculosis model, the absence of homeostatic chemokines delays granuloma formation and protective immunity. J Immunol 2009; 183:8004–14.
25. Kohlmeier JE, Reiley WW, Perona-Wright G, Freeman ML, Yager EJ, Connor LM, et al. Inflammatory chemokine receptors regulate CD8(+) T cell contraction and memory generation following infection. J Exp Med 2011; 208:1621–34.
26. Slight SR, Rangel-Moreno J, Gopal R, Lin Y, Fallert-Junecko BA, Mehra S, et al. CXCR5(+) T helper cells mediate protective immunity against tuberculosis. J Clin Invest 2013; 123:712–26.
27. Hamada H, Bassity E, Flies A, Strutt TM, Garcia-Hernandez M de L, McKinstry KK, et al. Multiple redundant effector mechanisms of CD8+ T cells protect against influenza infection. J Immunol 2013; 190:296–306.
28. Mikhak Z, Strassner JP, Luster AD. Lung dendritic cells imprint T cell lung homing and promote lung immunity through the chemokine receptor CCR4. J Exp Med 2013; 210:1855–69.
29. Crotty S. T follicular helper cell differentiation, function, and roles in disease. Immunity 2014; 41:529–42.
30. Webster B, Ekland EH, Agle LM, Chyou S, Ruggieri R, Lu TT. Regulation of lymph node vascular growth by dendritic cells. J Exp Med 2006; 203:1903–13.
31. Liu C, Lin J, Zhao L, Yang Y, Gao F, Li B, et al. Gamma-ray irradiation impairs dendritic cell migration to CCL19 by down-regulation of CCR7 and induction of cell apoptosis. Int J Biol Sci 2011; 7:168–79.
32. Shulman Z, Gitlin AD, Targ S, Jankovic M, Pasqual G, Nussenzweig MC, et al. T follicular helper cell dynamics in germinal centers. Science 2013; 341:673–7.
33. Chyou S, Benahmed F, Chen J, Kumar V, Tian S, Lipp M, et al. Coordinated regulation of lymph node vascular-stromal growth first by CD11c+ cells and then by T and B cells. J Immunol 2011; 187:5558–67.
34. Cao MD, Chen ZD, Xing Y. Gamma irradiation of human dendritic cells influences proliferation and cytokine profile of T cells in autologous mixed lymphocyte reaction. Cell Biol Int 2004; 28:223–8.
35. Heylmann D, Rodel F, Kindler T, Kaina B. Radiation sensitivity of human and murine peripheral blood lymphocytes, stem and progenitor cells. Biochim Biophys Acta 2014; 1846:121–9.
36. Cyster JG, Ansel KM, Reif K, Ekland EH, Hyman PL, Tang HL, et al. Follicular stromal cells and lymphocyte homing to follicles. Immunol Rev 2000; 176:181–93.
37. Wolber FM, Leonard E, Michael S, Orschell-Traycoff CM, Yoder MC, Srour EF. Roles of spleen and liver in development of the murine hematopoietic system. Exp Hematol 2002; 30:1010–9.
38. McKinstry KK, Strutt TM, Swain SL. Hallmarks of CD4 T cell immunity against influenza. J Int Med 2011; 269:507–18.
39. Cao M, Cabrera R, Xu Y, Liu C, Nelson D. Different radiosensitivity of CD4(+)CD25(+) regulatory T cells and effector T cells to low dose gamma irradiation in vitro. Int J Radiat Biol 2011; 87:71–80.
40. Lim HW, Hillsamer P, Kim CH. Regulatory T cells can migrate to follicles upon T cell activation and suppress GC-Th cells and GC-Th cell-driven B cell responses. J Clin Invest 2004; 114:1640–9.
41. Linterman MA, Liston A, Vinuesa CG. T-follicular helper cell differentiation and the co-option of this pathway by non-helper cells. Immunol Rev 2012; 247:143–59.
42. Flynn KJ, Belz GT, Altman JD, Ahmed R, Woodland DL, Doherty PC. Virus-specific CD8+ T cells in primary and secondary influenza pneumonia. Immunity 1998; 8:683–91.
43. Kulkarni AA, Thatcher TH, Hsiao HM, Olsen KC, Kottman RM, Morrissette J, et al. The triterpenoid CDDO-Me inhibits bleomycin-induced lung inflammation and fibrosis. PloS One 2013; 8:e63798.
44. Franko AJ, Sharplin J. Development of fibrosis after lung irradiation in relation to inflammation and lung function in a mouse strain prone to fibrosis. Radiat Res 1994; 140:347–55.
45. Williams JP, Brown SL, Georges GE, Hauer-Jensen M, Hill RP, Huser AK, et al. Animal models for medical countermeasures to radiation exposure. Radiat Res 2010; 173:557–78.
46. Day RM, Snow AL, Panganiban RA. Radiation-induced accelerated senescence. A fate worse than death? Cell Cycle 2014; 13:2011–2.